Published in final edited form as:

Magn Reson Med. 2017 July ; 78(1): 387–398. doi:10.1002/mrm.26339.

Design and Implementation of Embedded 8-Channel Receive-Only Arrays for Whole-Brain MRI and fMRI of Conscious Awake Marmosets

Daniel Papoti[1], **Cecil Chern-Chyi Yen**[1], **Chia-Chun Hung**[1,2], **Jennifer Ciuchta**[1], **David A. Leopold**[2], and **Afonso C. Silva**[1,*]

[1]Cerebral Microcirculation Section, Laboratory of Functional and Molecular Imaging, National Institute of Neurological Disorders and Stroke, Bethesda, MD, 20892 USA

[2]Section on Cognitive Neurophysiology and Imaging, Laboratory of Neuropsychology, National Institute of Mental Health, National Institutes of Health, Bethesda, MD, 20892 USA

Abstract

Purpose—The common marmoset (Callithrix jacchus) is a New World primate of increasing interest to neuroscience and in translational brain research. The present work describes the design and implementation of individualized 8-channel receive-only RF coil arrays that provide whole brain coverage and allow anatomical and functional MRI experiments in conscious, awake marmosets.

Methods—The coil arrays were designed with their elements embedded inside individualized restraint helmets. The size, geometry and arrangement of the coil elements were optimized to allow whole brain coverage. Coil-to-coil decoupling was achieved by a combination of geometric decoupling and low input impedance preamplifiers. The performance of the embedded arrays was compared against that of one 8-channel receive-only array built to fit the external surface of the helmets.

Results—Three individualized helmets with embedded coil arrays were built for 3 marmosets. Whole-brain coverage was achieved with high sensitivity extending over the entire cortex. Visual stimulation of conscious awake marmosets elicited robust BOLD fMRI responses in both primary and higher order visual areas of the occipitotemporal cortex.

Conclusion—The high sensitivity provided by embedded receive-only coil arrays allows both anatomical and functional MRI data to be obtained with high spatial resolution in conscious, awake marmosets.

Keywords

non-human primates; functional magnetic resonance imaging; MRI phased arrays; receive-only RF coils; embedded RF coils

[*]Corresponding author. Afonso C. Silva - SilvaA@ninds.nih.gov, Address for correspondence: 49 Convent Drive MSC 4478, Building 49, Room 3A72, Bethesda, MD 20892-4478 USA, Phone: 301-402-9703, Fax: 301-480-8670.

Introduction

Since the early 1990s, functional Magnetic Resonance Imaging (fMRI) has established itself as one of the most used techniques in cognitive neuroscience[1]. Due to their close phylogenetic proximity to humans, nonhuman primates have an important role in basic and translational biomedical research[2]. Among nonhuman primates used in neuroscience research, Old World monkeys, including the various species of the genus *Macaca* are the most widely used to understand vision[3]. On the other hand, New World monkeys, including common marmosets (*Callithrix Jacchus*), are becoming an attractive model for biomedical research[4–6] and in neuroscience. Marmosets have many practical advantages over Old World primates, including excellent reproduction in captivity, quick development and sexual maturity achieved by 18 months, and enhanced biosafety[7]. In addition, several publications[8–13] have demonstrated that marmosets exhibit the typical primate anatomical and functional brain organization, featuring a well-developed prefrontal cortex, and specializations of the eye and brain that are in close homology to macaques and humans. Thus, it is important to develop neuroimaging techniques and devices to study the marmoset brain. A particular need is to develop radiofrequency (RF) coil arrays to enable anatomical and functional MRI data to be obtained from marmosets. To the best of our knowledge, currently there are no commercially available RF coils designed specifically for imaging the marmoset brain.

Marmosets can be trained to be temporarily restrained and thus participate in experiments that require immobilization, such as most neuroimaging experiments. One traditional way to restrain animals is through the use of anesthesia, which is quite effective for minimizing movements[11]. However, anesthesia is incompatible with measuring important aspects of cognition. Not only does anesthesia prevent animals from perceiving and interacting their environment, but also it interferes directly with both neural excitability and neurovascular coupling[14–17]. To overcome these disadvantages, we have previously devised a completely non-invasive method for restraining head motion in marmosets undergoing anatomical and/or functional MRI studies[14,18]. The method consists of acclimating marmosets to lie in the sphinx position in an MRI-compatible cradle, and having them wear individualized 3D printed helmets that constrain head motion with great comfort[14,18].

We describe here the design of individualized, 8-element receive-only RF coil arrays, in which the coil elements are built using flat conductors and placed on the inner surface of individualized restraining helmets to maximize the sensitivity of MRI and fMRI experiments at 7T in conscious awake marmosets while preserving comfort to the animals. The size, geometry and arrangement of the coil elements were optimized to allow whole-brain coverage, allowing us to obtain robust blood oxygenation level dependent (BOLD) fMRI responses to visual stimulation in both primary and higher order visual areas extending from the occipital lobe to the inferior temporal cortex. Finally, to investigate the advantages of producing individualized arrays embedded into individualized helmets, their performance was compared against that of a single 8-channel receive-only RF coil array built to fit the common external surface of the helmets. The sensitivity of the embedded arrays was remarkably higher than that of the external array, making this design a better choice for high resolution, whole-brain anatomical and functional MRI of the marmoset.

Methods

Individualized movement restraining helmets

Individualized movement restraining helmets were 3D-printed (Fortus 360mc, Stratasys, Inc., Eden Prairie, MN, USA)) out of polycarbonate. The helmets inner surfaces were shaped using individual marmoset head profiles obtained from 3D gradient echo images of the anesthetized marmosets head and torso, acquired using a custom built linearly driven 16-rung birdcage coil with 10 cm inner diameter operating as a transceiver. The parameters used during the 3D acquisition were: field of view (FOV) = 76.8 × 76.8 × 76.8 mm^3; matrix size = 160 × 160 × 160; echo time (TE) = 1.7 ms; repetition time (TR) = 15 ms and 4 averages, resulting in a total acquisition time of 25.6 min. Segmentation of the data was performed using the software ITK-SNAP[19] (University of Pennsylvania, Philadelphia, PA, USA), resulting in a 3D mesh profile which was imported into the 3D modeling program Solid Works (Waltham, Massachusetts, USA). The head profiles were expanded by 3 mm in all directions, to make space for placing compressible foam so as to provide additional comfort for the animals during the experiments. The individualized helmet inner surfaces were then obtained by subtracting the expanded head profiles using Boolean operations. As shown in Fig. 1 and Fig. 2, the helmets are composed of two parts. The top part holds most of the animal's head. The bottom piece supports the chin of the animal while allowing the animal enough room to lick and swallow liquid rewards during fMRI experiments. Fixation parts were added to both parts to attach the helmets to the cradle holding the marmosets.

Three adult male marmosets participated in this study, and two types of helmets were built for each marmoset, one for the individualized embedded array, and one for the common external RF coil array. The helmets for the 8-channel embedded arrays, where the coil elements were placed in the inner surface, were designed with a flat surface on top in order to house the circuit board made of flame retardant FR4, which includes the matching network and cable traps for every channel (Fig. 1a). The helmets used for the external 8-channel array were designed with a curved surface with a polycarbonate wall thickness of approximately 2 mm, following the contour of the marmoset's head (Fig. 2a). This was the minimum thickness that still provided enough mechanical support during the experiments for the helmets printed out from polycarbonate. This helmet design uses an external surface that is common for all marmosets' heads, and an internal surface that is still individualized for optimum movement restraint. The common external surface of the helmet allowed the same external coil array to be used with different marmosets.

8-channel embedded coil arrays

The 8-channel receive-only embedded coil arrays were built using CuFlon (Polyflon, Inc., Norwalk, CT, USA) with 610 g/m^2 of copper deposited in a 0.25 mm thick polytetrafluorethylene dielectric. This flexible and thin material made it possible to place each loop element of the array on the inner surface of the helmet with flat surface (Fig. 1d), which was then covered by 3-mm thick polyurethane foam to provide electrical isolation and additional comfort to the animal. Because foam gets compressed when the helmet is in place, the distance from coil elements to animal's head was approximately 2 mm. The coil layout (Fig. 1b, d) consisted of arranging the elements in two frontal rows of 3 elements,

overlapped in the head-foot (Z) direction and gapped in left-right (X) direction, and placed over the pre-frontal and parietal cortices, respectively. Two additional elements, overlapped in the X direction, were placed in the back of the array over the occipital cortex. This design was chosen as a compromise between achieving whole brain coverage, high sensitivity over the cortex, and to allow the possibility of performing parallel imaging in some MRI and fMRI protocols that needed faster acquisition times. The inner diameter of each circular loop in the front is 15 mm and 12 mm for the loops in the back, and the copper width is 1.5 mm. The connection between the coil elements and the FR4 circuit board having all eight matching networks (Fig. 1c), placed on the top of the flat surface of the helmets, were made by soldering copper wire with 0.64 mm diameter (AWG 22) through the helmet's polycarbonate wall. The coil circuitry for each coil element (Fig. 3) consisted of a matching network and a PIN diode controlled blocking circuit for active detuning during transmission[18]. To detune the coil during the transmit period, a blocking circuit consisting of C_3 and L_d was activated by providing DC current to the PIN diode via a bias T located in the same circuit board that houses the low-input-impedance preamplifiers. The components used for the tuning/matching network consisted of non-magnetic chip capacitors (A series, American Technical Ceramics, Huntington Station, NY, USA), air core inductors (micro-spring air core inductors, Coilcraft, Cary, IL, USA) and PIN diodes (Temex Ceramics, Pessac, France). The main decoupling mechanism was achieved by connecting each individual element to a low input impedance preamplifier[20,21]. The total phase of each element, including the coaxial cable and the preamplifier, was adjusted by careful trimming of the cable length. Partial geometrical overlapping along the Z direction improved decoupling between elements in the 2 front rows and those in the back row. To avoid cross-talk interactions between the RF coaxial cables, cable traps[22] were placed in between the matching network and the input of the preamplifiers, and tuned to 300.4 MHz.

8-channel external array

To compare the advantages obtained by embedding the coil elements in the inner surface of the customized movement restraint helmets, an 8-channel receive-only array was built to fit the common external surface of the helmets (Fig. 2a). This external array was designed after the embedded arrays were in use, and we aimed for a universal design that could be used with different marmosets and yet one that provided at least the same spatial coverage and penetration depth in the brain as the embedded coil arrays, while still maintaining high SNR in the cortex. In the external array, the coil elements had to be placed on the external surface of the restraint helmets, and because they would be further away from the marmosets' brains, the elements were made bigger. Due to the limited number of RF receivers, it was not possible to resort to fully symmetric designs, such as the soccer ball[23]. Therefore, we chose the design of 2×4 elements overlapped in both X and Z directions to achieve whole brain coverage (Fig. 2b). The coil loops were mounted and fixed using hot glue onto a 3D printed polycarbonate support shell with 1 mm thick that matched the external surface of the helmets. When the external array was positioned on the helmets, the distance between coil elements and the marmoset's head was approximately 5 mm. Since there was no space constraint, instead of flat and flexible conductors this coil was built using copper wire of 1.4 mm outer diameter (AWG 16) to provide a higher quality factor (Q) for each coil element by reducing the resistive losses in the conductor.

To allow the coil wires to cross over without touching the nearest neighbor elements, semicircular bridges were bent into the loop wires, as suggested by Keil et al.[24,25] (Fig. 2d). Each element was built as a circle with a 25 mm inner diameter, except for the 2 outer elements in the front row. These elements were built as ellipses with 25 mm and 30 mm to cover the entire external surface of the helmet, allowing the coil sensitivity to extend through the temporalis muscle and reach into the temporal lobe of the marmoset brain. The coil circuitry of each element was essentially the same as those used in the 8-channel embedded array (Fig. 3), with the exception that individual floating bazookas were used as cable traps[22] over each individual coaxial cable.

Low input impedance preamplifiers

Preamplifier decoupling was achieved by connecting either 8-channel receive array to home built low input impedance preamplifiers[26,27]. The preamps were designed with an input impedance of approximately 1.0 Ω, gain of 32 dB and noise figure of 0.6 dB. The set of eight preamps were arranged in two layers with 4 preamps each, using non-magnetic MCX connectors to connect both 8-channel coil arrays. All preamps were mounted to motherboards (4 preamps per motherboard) and placed inside a 3D printed box (2 motherboards per box) that could be fixed in the animal's cradle during the experiments. The coil elements were detuned by DC current provided to the PIN diodes via a bias T located in the same FR4 motherboards where the preamps were mounted.

Characterization on the bench and SNR maps

Characterization of both receive arrays was performed on the bench by measuring S-parameters using a network analyzer (Agilent Technology, Santa Clara, CA, USA) and a homemade detuning box providing 10 V/100 mA to bias the PIN diodes during the transmit mode and −30 V during the receive mode[24,25]. This box allowed us to bias the PIN diodes to evaluate the coil elements individually while all other elements remained detuned. Additionally, it provided 10V/130 mA to power the low input impedance preamplifiers. Both 8-channel arrays were characterized by evaluating the detuning efficiency provided by the active detuning network, and the isolation due to preamplifier decoupling. For all measurements of the transmission coefficients S_{21}, a probe consisting of a geometrically decoupled (> 75 dB isolation) pair of overlapped pick-up loops was used. The probe consisted of two loops with 5 mm inner diameter each made of semi-rigid coaxial cables with a gap in the shield placed symmetrically at the center of each loop. Tuning of each element in the array was optimized by measuring the S_{21} response using the pick-up loops with the coil loaded while all other elements not under test were actively detuned. The isolation provided by the active detuning network was determined by the change in S_{21} response for an array element with and without forward bias current in the PIN diode. Again, during the measurements the elements not under test remained detuned by providing DC current to the PIN diodes, activating the blocking network. The isolation due to preamplifier decoupling was evaluated by measuring the difference in S_{21} responses when the element under test was power matched (i.e., 50 Ω terminated) and in the case when the coil was noise matched (low input impedance preamplifier termination[21,28]). To evaluate losses introduced by the sample and coil circuitry, the ratio of quality factor unloaded-to-loaded (Q_U/Q_L) was measured using a 3D printed phantom with a marmoset's head shape

filled with 9 g/L of sodium chloride solution. Q measurements were performed for each isolated element, without coaxial cables or preamplifiers connected. To ensure just the necessary coupling from the pickup loops to the coil under test, we tried to position the pick-up loops such that the baseline of the S_{21} curve was always around −70 dB, which was achieved by placing the probe approximately 2.5 cm away from the element under test. Q values were measured directly with the network analyzer function BANDWIDTH ON at −3dB, which acquired the bandwidth (Δf_{-3dB}) at −3 dB and directly displayed the ratio $f_0/\Delta f_{-3dB}$, where f_0 is the center frequency. During the measurements, the loops not under test remained actively detuned by forward biasing the PIN diodes with DC current using the detuning box described above. Please see[25,28,29] for further detailed information about how the workbench measurements were performed.

Coil performance in the scanner

All imaging experiments were performed in a 7T Ultra Shielded Refrigerated magnet (Bruker-Biospin, Inc. Ettingen, Germany) with a 30 cm bore equipped with 8 RF receivers connected to an AVIII console running ParaVision 5.1. A custom-built 16-rung transmit-only linearly driven birdcage coil was used for excitation. Both transmit RF coil and the 8-element receive arrays were equipped with actively detuning circuits, so that the receive arrays were detuned during transmission and the volume transmit-only RF coil was switched off during reception. The good performance provided by the detuning network of the transmit-only RF coil used here was verified by comparing B1 maps with and without the presence of a receive array at the center of the coil, as previously described[18].

To verify coil-to-coil isolation, noise correlation matrices were acquired for both coil arrays placed on the heads of the marmosets. The noise correlation matrix between the ith and jth coil receive elements was computed using $\psi_{ij}^{\mathrm{corr}}=\psi_{ij}/(\psi_{ii}\psi_{jj})^{1/2}$, where ψ_{ij} is the noise covariance matrix, which is calculated from $\psi_{ij}=\langle n_i \cdot n_j^* \rangle$ where n_i e n_j are the complex noise variances from noise images acquired without RF excitation[25].

Signal-to-Noise ratio (SNR) maps from both 8-channel arrays were acquired from a conscious awake marmoset using a fast low angle shot (FLASH) sequence with TR = 700 ms, TE = 4.2 ms, FOV = 38.4 × 38.4 mm^2, slice thickness = 2 mm, matrix = 256 × 256 and 2 averages, resulting in a total scan time of 5 min 58 s.

The noise amplification due to generalized auto calibrating partially parallel acquisitions (GRAPPA) accelerated images was evaluated by computing g-factor maps[30] using a custom software written in MATLAB (MathWorks Inc. Natick, MA, USA). For these measurements, both coils were loaded with the same phantom used for Q measurements, with acceleration factors of R = 2, 3, 4 in the head-foot (Z) and left-right (X) directions. The images for g-factor maps calculation were acquired in coronal orientation in a plane located 20 mm from the inner surface of the helmets, which is approximately the position of the center of a marmoset's head, using Rapid Acquisition with Relaxation Enhancement (RARE) with 8 echoes, TR = 700 ms, TE = 4.4 ms, FOV = 51.2 × 51.2 mm^2, slice thickness = 1 mm, matrix = 128 × 128 and 2 averages.

fMRI experiments in response to visual stimulation in conscious awake marmosets

All experiments were performed in accordance to guidelines set by the Animal Care and Use Committee of the National Institute of Neurological Disorders and Stroke. Detailed fMRI procedures are described in two previous publications[31,32]. Briefly, fMRI experiments in response to visual stimulation were performed in two adult male marmosets previously acclimated to the restraint helmets and to MRI sounds[14,32]. For visual stimulation, five different image stimulus categories: conspecific faces, conspecific body parts, man-made objects, and spatially and phase scrambled images, were presented via a LCD monitor (Tech Video System Co., Ltd, Suzhou, China) installed in the back of the magnet[31,32]. An additional fixation-only block, in which only a small fixation dot is shown at the center of the screen, was used as a control. The animals were trained to maintain their gaze on the images. The gaze was monitored via video-based eye tracking with an MR-compatible camera and infrared light illumination (Model 12M-i, MRC Systems, GmbH, Heidelberg, Germany) (Fig. 4). Liquid rewards for task compliance were delivered through a plastic tube positioned in the animal's mouth. BOLD fMRI data from 18 axial slices were obtained using a 2D gradient-recalled echo planar imaging (EPI) sequence with TR = 2000 ms, TE = 26 ms, thickness = 1 mm, FOV = 32 × 32 mm^2, matrix 64 × 64, acceleration factor (R = 2) in the head-foot (Z) direction and GRAPPA reconstruction. During each run, 512 volumes were acquired. Parallel acceleration of EPI was essential to reduce signal dropouts induced by susceptibility artifacts near the occipital and temporal lobes and to increase the number of slices without running into gradient duty cycle limitations. Coplanar T_2 weighted anatomical images ($TE_{effective}$ = 64 ms; TR = 4000 ms; FOV = 32 × 32 mm^2; slice thickness = 1 mm; matrix = 128 × 128) were collected per session for image registration. Visual stimuli of the same category extending 5° visual angle were randomly displayed every 500 ms throughout the 16 s blocks. A fixed inter-block interval of 20 s of uniform gray screen was used. Analysis of the fMRI data acquired was performed using the software Analysis of Functional Neuroimages (AFNI)[33], and custom code written in MATLAB (The Mathworks, Natick, MA, USA). Data analysis was restricted to only those blocks in which the subject's gaze remained within a 5° radius window more than 80% (12.8 s out of 16 s) of the block duration. Visual responses, including visual selectivity, were based on analysis of volumes collected between 4 and 18 seconds after stimulus onset. Statistical tests for stimulus selectivity during this period were based on two-sample t-test with correction for multiple comparisons. Group averaged BOLD response time courses of four categories (faces, bodies/objects, phase/spatial scrambled faces and fixation dot) were plotted by averaging across sessions and animals. Voxels with t-value > 5 for the contrast between face and fixation dot were clustered together for averaging. The error bar in the time courses indicated one standard error across block repetitions.

Results

Characterization on the bench

Fig. 5a–b show S-parameter matrices measured on the bench for the 8-channel embedded array and for the 8-channel external array, respectively. For the 8-channel embedded array, the active detuning isolation averaged −32 dB (range −28 dB to −36 dB). Reflection coefficients, shown by the diagonal elements of Fig. 5a, averaged −12 dB (range −8 dB to

−17 dB). Decoupling between nearest neighbor elements, achieved by partial geometrical overlapping, averaged −8 dB (range −4 dB to −12 dB). This unexpected low decoupling value was probably due to difficulties in properly positioning the pickup loops over the coil elements while simultaneously moving the elements to their optimal overlap position. The use of low input preamplifiers improved the coil-to-coil decoupling by an additional −26 dB, on average.

The same workbench measurements were performed on the 8-channel external array. The active detuning isolation averaged −36 dB (range −32 dB to −39 dB). Reflection coefficients, shown by the diagonal elements of Fig. 5b, averaged −12 dB (range −9 dB to −16 dB). Decoupling between nearest neighbor elements averaged −16 dB (range −11 dB to −19 dB). In this case, the achieved decoupling was better because it was easier to find the optimal overlap position of the individual elements, since they were placed outside the helmets. On average, an additional isolation of −30 dB was provided by the use of low-input impedance preamplifiers.

For the embedded array, Q ratio measurements of a typical element were Q_u/Q_L = (142/100) = 1.42, and the average value across all elements was 1.43 ± 0.25. For the external array, the Q ratio of a typical element was Q_u/Q_L = (138/107) = 1.29, and the average value across all elements was 1.31 ± 0.13. These measurements show that the two arrays are roughly equivalent from the noise point of view. The embedded array has smaller elements, but these elements are positioned closer (~3 mm) to the sample than the external array, which has larger coil elements, but positioned further away (~5 mm) from the sample. Therefore, for both designs, coil resistance – and not sample noise – constitutes the main source of noise.

Coil performance in the scanner

Fig. 5c–d show noise correlation matrices obtained for both coils calculated from images acquired without RF excitation for both receive arrays, where the elements on the diagonal of the matrix represent the noise level with its average normalized to 1. For the 8-channel embedded array, the largest off-diagonal correlation coefficient was 0.52 with an average of 0.25 (Fig. 5c). The noise level range represented by the diagonal elements was 0.32 – 1.33. For the 8-channel external coil, the largest correlation coefficient was 0.70, and an average of 0.26 (Fig. 5d), with the noise level ranging 0.24 – 1.79.

SNR maps obtained in axial, coronal and sagittal orientations were calculated from images acquired from a conscious awake marmoset and are displayed in Fig. 6. The 8-channel embedded array provides high sensitivity along the entire cortical brain surface, with only a slight loss of sensitivity in the frontal cortex. The mean SNR gain obtained when comparing the embedded array with the external array was calculated inside ROIs in the cortex and at the center of the brain, as defined in each of the 3 main spatial orientations (Fig. 6). In the axial orientation (Fig. 6a), the embedded array had an average 20% higher SNR in the cortex and 4% higher in the center of brain when compared to the external array. In the coronal orientation (Fig. 6b), the SNR measured in the occipital cortex was 65% higher for the embedded array. At the center, the gain was 31% higher. In the sagittal orientation (Fig. 6c), the SNR of the embedded array was 36% higher in the cortex, and only 0.5 % higher at the center. Interestingly, in deeper brain structures the performances of the two coil arrays were

roughly equivalent. Thus, the main advantage of the embedded arrays was found in the occipital cortex.

Fig. 7 shows noise amplification (g-factor) maps obtained when performing parallel imaging experiments, with table 1 summarizing the measured g-factor (mean ± standard deviation, and the maximum value) over the phantom for both coil designs. For the 8-channel embedded array, the g-factor maps (Fig. 7a) indicate that the preferred direction for acceleration is L-R (X). This result was expected for gapped coil geometries[34,35] since there is a 1 mm gap between the elements in this direction. For the 8-channel external array (Fig. 7b), all coils overlap in both L-R (X) and H-F (Z) directions. But because the external array only has 2 rows in the H-F direction, the preferred direction for parallel imaging acceleration is L-R. This can be seen from the quicker deterioration of the g-factor maps (Table 1) with increasing R in the H-F direction (Fig. 7b) compared to Fig. 7a.

fMRI experiments

The performance of the 8-channel embedded arrays was tested in fMRI experiments in 2 out of the 3 conscious, awake marmosets[31,32]. The 8-channel embedded arrays provided sufficient sensitivity throughout the entire cortex and most subcortical areas of the marmoset brain, which enabled differentiation of small BOLD fMRI signal differences across different conditions. For example, there was less than 1% difference in the BOLD response to the presentation of faces versus other types of visual stimuli and yet these differences could be readily detected in five distinct patches of the marmoset's occipitotemporal cortex[31,32]. In Fig. 8a–c, BOLD activation maps of faces versus objects are overlaid on skull-stripped axial (Fig. 8a) and coronal (Fig. 8b) T1-weighted anatomical images. Fig. 8c shows the same functional map overlaid on a surface-rendered template of the marmoset brain[36]. Slice positions are represented by two crossing red lines in Fig. 8c, which intersect at one of the five face patches. Although the marmoset's inferior temporal lobe sits in an unfavorable lateral and inferior position of the marmoset head, and is covered by the temporalis muscle on the side of the head, we were able to detect face patches in that region, owing to the sensitivity provided by the embedded arrays. Significant BOLD activation was seen over both occipitotemporal cortices (the left hemisphere is not shown in the figure). Group averaged BOLD fMRI time courses to four categories of visual stimuli are plotted in Fig. 8d. In this face patch, presentation of face visual stimuli elicited the highest BOLD response (~1.5% at peak) compared to the other three categories. Detection of differences between BOLD responses to faces versus objects (~0.5%), required stable and sensitive apparatus, like the aforementioned highly optimized embedded phase array.

Discussion and Conclusion

We have demonstrated the development of two different designs of 8-channel receive-only RF coil arrays for MRI and fMRI experiments in conscious, awake marmosets. For each of the 3 adult male common marmosets used in the present study, 2 restraint helmets were built, one for the embedded coil array, and one for the external coil array. In one design, RF coil arrays were built embedded onto the inner surface of the head restraint helmets in a way that minimizes the distance between the coil elements and the brain. This design showed

improved sensitivity over cortex at the cost of necessitating one array for each individualized helmet. In the other design, a single external RF coil array was built so that its coil elements could be placed on the common external surface of individualized head restraint helmets. This allowed the external array to be shared amongst all 3 individuals in the study, with the disadvantage that the coil elements were further away from the brain.

For both coil designs, the main coil-to-coil decoupling mechanism relies on the low input impedance preamplifiers, slightly improved by partial overlapping for some neighbor elements in each coil design. Even though the workbench measurements has shown isolation better than −26 dB provided by the combination of partial overlapping and preamplifiers decoupling, the noise correlation matrices (Fig. 5c–d) showed considerable level of coupling between some coil elements, where the highest coupling coefficient was verified between channels 6 and 8 in the external array design. This higher value is probably due to a misadjustment of the phase during the cable length trimming of those elements, which was hard to correct after the coil was tested in the scanner, since changing those particular cables would imply in changing the whole 8-channel cable. Furthermore, these high average values observed for the correlation coefficients in both coil designs could be attributed to the fact that some coil elements are not completely overlapped with their nearest neighbors. For instance, in the embedded array design (Fig. 5) there is a strong coupling between element 1 with its neighbors 2 and 5. For the external array design (Fig. 5), element 1 is strongly coupled with its neighbor element 6, for instance. Therefore, the choice of gapped design for the embedded array may be the reason for the high noise correlation coefficients. It is also important to point out that the noise correlation is not strictly depending on coil coupling, since fully decoupled coil elements can still have a high noise correlation, e.g. if they receive noise through the sample.

The characterization performed on the bench showed that the isolation provided by partially overlapping nearest neighbor elements in the embedded array (−8 dB) was considerably lower than the isolation achieved for the external array (−16 dB). In order to compensate for the low isolation achieved by geometric decoupling, we increased the value of the decoupling inductor L_d (as shown in Fig. 3) to increase the blocking impedance provided by the use of low input impedance preamplifiers, meaning that a better channel isolation due to preamplifier decoupling will be achieved. However, with the higher value of L_d, the coil will be slightly mismatched from 50 Ω. Nevertheless, this should not affect the SNR performance, as already pointed out by Keil et al[24].

The SNR maps comparison displayed in Fig. 6 shows that the 8-channel embedded coil provided higher SNR in the investigated regions of interest next to the cortex, providing the higher SNR gain over the occipital cortex, compared to the external array, as seen in the coronal orientation in Fig. 6b. This high SNR gain is due to the usage of two dedicated coil elements, placed directly over the occipital cortex, in high proximity to the brain. As expected, however, the SNR advantage of the embedded array disappeared in deeper brain structures, which are located far away from the coil elements. The comparison of the performance between both coil designs at the center of the brain shows a SNR gain of 4% considering the axial orientation (Fig. 6a) and 0.5% when considering the sagittal orientation (Fig. 6c). These results clearly show the advantage of using the embedded array for

achieving higher SNR in the cortex, making this design promising for fMRI experiments with focus on this region.

The mean g-factor values presented in Table 1 show that both coil designs allow parallel imaging experiments with acceleration factors of up to 2 without significant SNR degradation in the left-right (X) direction. In fact, for R = 2, the 8-channel embedded array allows acceleration in both directions (L-R and H-F) without significant drops in SNR. For R > 2, the advantage of the embedded array compared to the external array for parallel imaging experiments becomes even more prominent. Even though the 8-channel external array has 4 elements along the L-R (see coil layout in Fig. 2), the mean and maximum g-factor values are higher compared to the embedded array. For instance, in the L-R direction of acceleration for R = 3 the mean g-factor is 8% higher for the external array compared to the embedded array. This was an expected result, since the embedded array was designed with a 1 mm gap between the coil elements in this direction. On the other hand, the external array only allowed acceleration in the X direction, because it only features 2 columns in the H-F (Z) direction. Although parallel acceleration was done in the H-F direction (z-axis) due to susceptibility artifact in left-right direction for our fMRI experiment, the 8-channel embedded array would allow parallel imaging experiments with acceleration factors of up to 2 without high SNR degradation in the H-F direction.

fMRI experiments in response to visual stimulation were performed in 2 awake behaving marmosets using the 8-channel embedded arrays (Fig. 4)[31,32]. With the high SNR provided by the embedded receive arrays, we were able to demonstrate robust visual responses in both cortical and subcortical visual areas[32] and mapped discrete face processing areas in the extrastriate cortex of the common marmoset[33]. The spatial correspondence of the identified face patches[31,37] is in accordance to what is found in macaques and humans[37,38]. It is suggested that the two most anterior face patches along the marmoset ventral visual steam are similar in position to the macaque middle and anterior face patches, respectively. Our 8-channel embedded array allowed for mapping of functional regions in the inferior temporal lobe of the marmoset with high sensitivity, showing this design is suitable for looking at long-range functional areas involved in visual perception, e.g. from V1 to extrastriate and pre-frontal and frontal cortices.

In conclusion, the 8-channel embedded arrays showed high whole-brain coverage and enhanced SNR in the cortex. The main disadvantage of this design is that each animal requires its own array to be built together with the individualized movement restraining helmet. This becomes burdensome and inconvenient in studies that utilize a large number of animals. On the other hand, the 8-channel external array is a design suitable for being shared amongst different animals, but it cannot achieve the same imaging performance concerning SNR in the cortex and acceleration capabilities.

Acknowledgments

The authors are grateful to Xianfeng (Lisa) Zhang for her excellent technical skills, and to Dr. Stephen Dodd for his help with assembly of the preamplifiers. This research was supported by the Intramural Research Program of the NIH, NINDS and partially supported by the Brazilian National Council for Scientific and Technological Development (CNPq), through a Science without Borders Program fellowship (process # 207982/2012-0) to Daniel Papoti.

References

1. Poldrack RA. The role of fMRI in cognitive neuroscience: where do we stand? Curr Opin Neurobiol. 2008; 18(2):223–227. [PubMed: 18678252]
2. Capitanio JP, Emborg ME. Contributions of non-human primates to neuroscience research. Lancet. 2008; 371(9618):1126–1135. [PubMed: 18374844]
3. Rosa MG, Tweedale R. The dorsomedial visual areas in New World and Old World monkeys: homology and function. Eur J Neurosci. 2001; 13(3):421–427. [PubMed: 11168549]
4. Kishi N, Sato K, Sasaki E, Okano H. Common marmoset as a new model animal for neuroscience research and genome editing technology. Development Growth & Differentiation. 2014; 56(1):53–62.
5. Okano H, Hikishima K, Iriki A, Sasaki E. The common marmoset as a novel animal model system for biomedical and neuroscience research applications. Seminars in Fetal & Neonatal Medicine. 2012; 17(6):336–340. [PubMed: 22871417]
6. Solomon SG, Rosa MG. A simpler primate brain: the visual system of the marmoset monkey. Front Neural Circuits. 2014; 8:96. [PubMed: 25152716]
7. Mansfield K. Marmoset models commonly used in biomedical research. Comp Med. 2003; 53(4): 383–392. [PubMed: 14524414]
8. Cheong SK, Tailby C, Solomon SG, Martin PR. Cortical-like receptive fields in the lateral geniculate nucleus of marmoset monkeys. J Neurosci. 2013; 33(16):6864–6876. [PubMed: 23595745]
9. Mitchell JF, Leopold DA. The marmoset monkey as a model for visual neuroscience. Neurosci Res. 2015; 93:20–46. [PubMed: 25683292]
10. Rosa MG, Tweedale R. Brain maps, great and small: lessons from comparative studies of primate visual cortical organization. Philos Trans R Soc Lond B Biol Sci. 2005; 360(1456):665–691. [PubMed: 15937007]
11. Liu JV, Hirano Y, Nascimento GC, Stefanovic B, Leopold DA, Silva AC. fMRI in the awake marmoset: somatosensory-evoked responses, functional connectivity, and comparison with propofol anesthesia. Neuroimage. 2013; 78:186–195. [PubMed: 23571417]
12. McDonald JS, Clifford CW, Solomon SS, Chen SC, Solomon SG. Integration and segregation of multiple motion signals by neurons in area MT of primate. J Neurophysiol. 2014; 111(2):369–378. [PubMed: 24155007]
13. Yu HH, Rosa MG. Uniformity and diversity of response properties of neurons in the primary visual cortex: selectivity for orientation, direction of motion, and stimulus size from center to far periphery. Vis Neurosci. 2014; 31(1):85–98. [PubMed: 24160942]
14. Silva AC, Liu JV, Hirano Y, Leoni RF, Merkle H, Mackel JB, Zhang XF, Nascimento GC, Stefanovic B. Longitudinal functional magnetic resonance imaging in animal models. Methods Mol Biol. 2011; 711:281–302. [PubMed: 21279608]
15. Masamoto K, Kim T, Fukuda M, Wang P, Kim SG. Relationship between neural, vascular, and BOLD signals in isoflurane-anesthetized rat somatosensory cortex. Cerebral Cortex. 2007; 17(4): 942–950. [PubMed: 16731882]
16. Masamoto K, Fukuda M, Vazquez A, Kim SG. Dose-dependent effect of isoflurane on neurovascular coupling in rat cerebral cortex. Eur J Neurosci. 2009; 30(2):242–250. [PubMed: 19659924]
17. Wegener S, Wong EC. Longitudinal MRI studies in the isoflurane-anesthetized rat: long-term effects of a short hypoxic episode on regulation of cerebral blood flow as assessed by pulsed arterial spin labelling. NMR Biomed. 2008; 21(7):696–703. [PubMed: 18275045]
18. Papoti D, Yen CC, Mackel JB, Merkle H, Silva AC. An embedded four-channel receive-only RF coil array for fMRI experiments of the somatosensory pathway in conscious awake marmosets. NMR Biomed. 2013; 26(11):1395–1402. [PubMed: 23696219]
19. Yushkevich PA, Piven J, Hazlett HC, Smith RG, Ho S, Gee JC, Gerig G. User-guided 3D active contour segmentation of anatomical structures: significantly improved efficiency and reliability. Neuroimage. 2006; 31(3):1116–1128. [PubMed: 16545965]

20. Roemer PB, Edelstein WA, Hayes CE, Souza SP, Mueller OM. The Nmr Phased-Array. Magnetic Resonance in Medicine. 1990; 16(2):192–225. [PubMed: 2266841]
21. Reykowski A, Wright SM, Porter JR. Design of matching networks for low noise preamplifiers. Magn Reson Med. 1995; 33(6):848–852. [PubMed: 7651124]
22. Seeber DA, Jevtic I, Menon A. Floating shield current suppression trap. Concepts in Magnetic Resonance Part B-Magnetic Resonance Engineering. 2004; 21b(1):26–31.
23. Wiggins GC, Triantafyllou C, Potthast A, Reykowski A, Nittka M, Wald LL. 32-channel 3 Tesla receive-only phased-array head coil with soccer-ball element geometry. Magn Reson Med. 2006; 56(1):216–223. [PubMed: 16767762]
24. Keil B, Wald LL. Massively parallel MRI detector arrays. J Magn Reson. 2013; 229:75–89. [PubMed: 23453758]
25. Keil B, Wiggins GC, Triantafyllou C, Wald LL, Meise FM, Schreiber LM, Klose KJ, Heverhagen JT. A 20-channel receive-only mouse array coil for a 3 T clinical MRI system. Magn Reson Med. 2011; 66(2):584–595. [PubMed: 21433066]
26. Nascimento, GC., Paiva, FF., Silva, AC. Inductive Decoupling of RF Coil Arrays: A Study at 7T; Proceedings of the 14th Annual Meeting of ISMRM; Seattle, USA. 2006. p. 2590
27. Dodd, SJ., Nascimento, GC., Hsieh, M-C., Merkle, H., Murphy-Boesch, J., Chen, J-H., Koretsky, AP., Silva, AC. Modular Preamplifier Design and Application to Animal Imaging at 7 and 11.7T; Proceedings of the 17th Annual Meeting of ISMRM, Honolulu; Hawaii, USA. 2009. p. 3141
28. Griswold, M. Characterization of multichannel coil arrays on the benchtop. Wiley: Encyclopedia of Magnetic Resonance; 2012.
29. Vaughan, JT., Griffiths, JR. RF coils for MRI. Chichester, West Sussex: John Wiley and Sons Ltd.; 2012. p. xvip. 452
30. Breuer FA, Kannengiesser SA, Blaimer M, Seiberlich N, Jakob PM, Griswold MA. General formulation for quantitative G-factor calculation in GRAPPA reconstructions. Magn Reson Med. 2009; 62(3):739–746. [PubMed: 19585608]
31. Hung CC, Yen CC, Ciuchta JL, Papoti D, Bock NA, Leopold DA, Silva AC. Functional Mapping of Face-Selective Regions in the Extrastriate Visual Cortex of the Marmoset. Journal of Neuroscience. 2015; 35(3):1160–1172. [PubMed: 25609630]
32. Hung CC, Yen CC, Ciuchta JL, Papoti D, Bock NA, Leopold DA, Silva AC. Functional MRI of visual responses in the awake, behaving marmoset. Neuroimage. 2015; 120:1–11. [PubMed: 26149609]
33. Cox RW. AFNI: software for analysis and visualization of functional magnetic resonance neuroimages. Comput Biomed Res. 1996; 29(3):162–173. [PubMed: 8812068]
34. de Zwart JA, Ledden PJ, Kellman P, van Gelderen P, Duyn JH. Design of a SENSE-optimized high-sensitivity MRI receive coil for brain imaging. Magn Reson Med. 2002; 47(6):1218–1227. [PubMed: 12111969]
35. Ohliger MA, Sodickson DK. An introduction to coil array design for parallel MRI. NMR Biomed. 2006; 19(3):300–315. [PubMed: 16705631]
36. Bock NA, Kocharyan A, Liu JV, Silva AC. Visualizing the entire cortical myelination pattern in marmosets with magnetic resonance imaging. J Neurosci Methods. 2009; 185(1):15–22. [PubMed: 19737577]
37. Tsao DY, Moeller S, Freiwald WA. Comparing face patch systems in macaques and humans. Proc Natl Acad Sci U S A. 2008; 105(49):19514–19519. [PubMed: 19033466]
38. Lafer-Sousa R, Conway BR. Parallel, multi-stage processing of colors, faces and shapes in macaque inferior temporal cortex. Nat Neurosci. 2013; 16(12):1870–1878. [PubMed: 24141314]

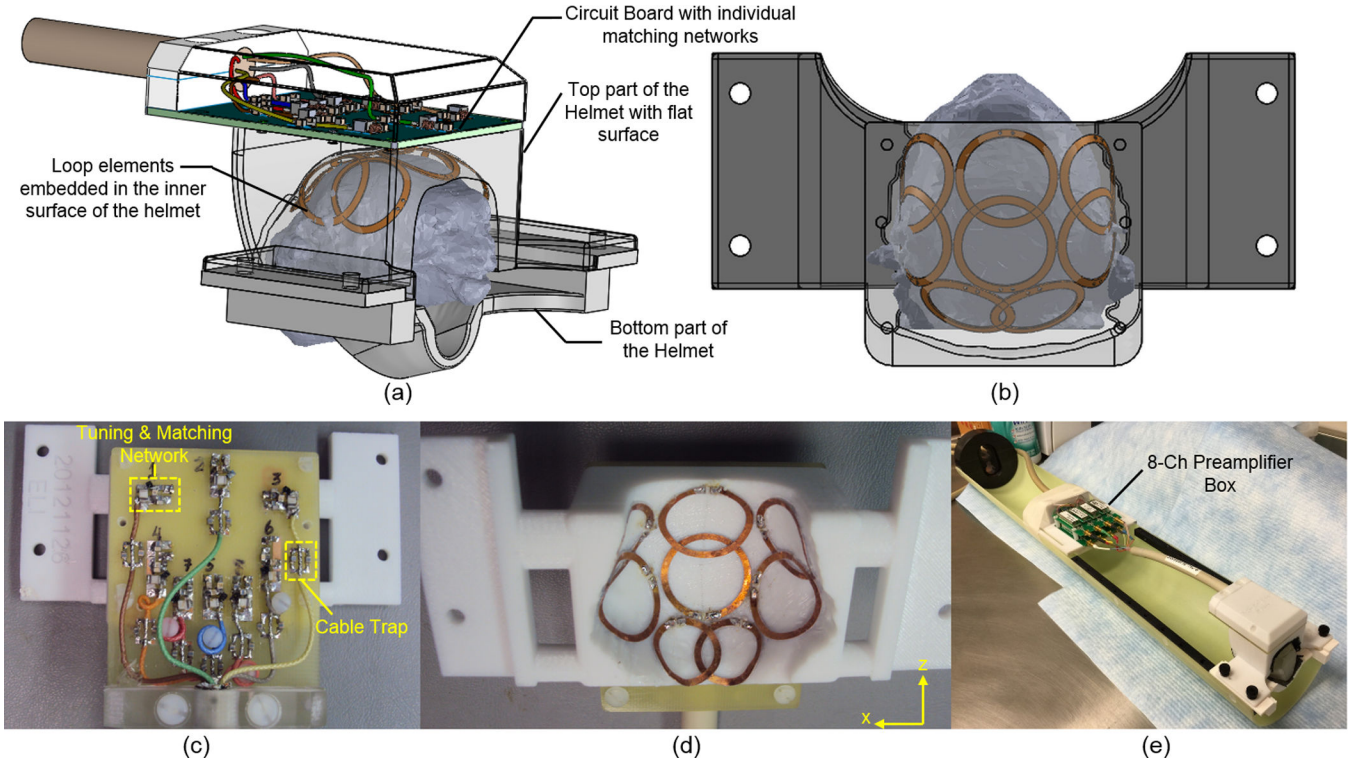

Figure 1.

(a) Individualized restraining helmets with flat surface designed for the 8-channel embedded arrays. The inner surface of the helmet conforms anatomically to the 3D profile of each individual's head. The bottom piece supports the chin of the animal while allowing the animal enough room to lick and swallow for liquid rewards. Because of the different individualized inner surfaces, each individual animal needs its own embedded array. (b) Layout of an 8-channel embedded array. (c) FR4 circuit board with the tuning/matching network and cable traps for each element in the 8-channel embedded array. (d) Picture of the coil layout with loop elements glued on the inner surface of the 3D printed helmet. (e) 8-channel embedded array loaded with a phantom and connected to the 8-channel preamplifier box.

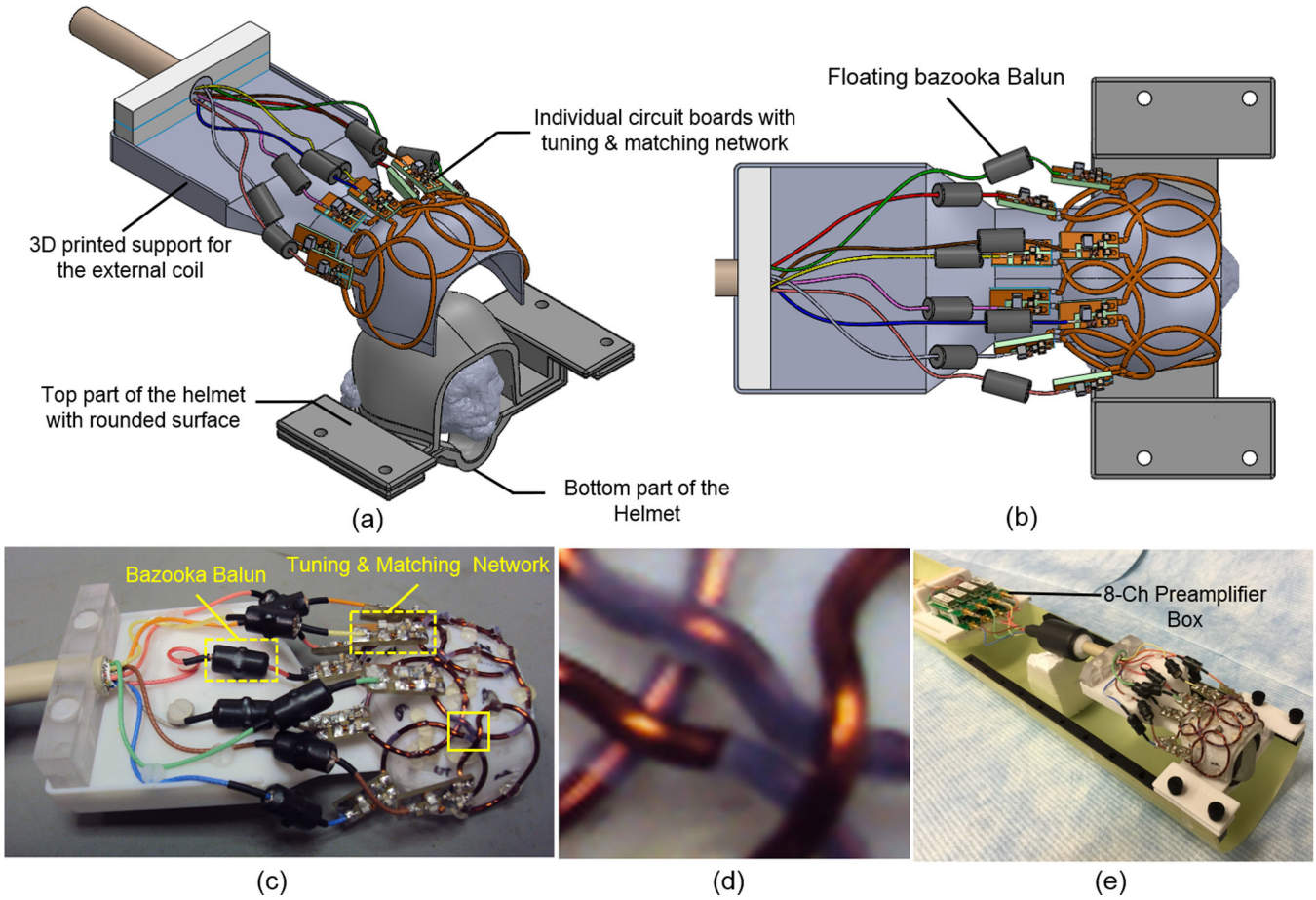

Figure 2.

(a) Individualized restraining helmets with curved surface designed for the 8-channel external array. A 3D printed coil support with inner surface that matches the external curved surface of the helmets was used to build the external array. Because the coil support fits into different individualized restraint helmets with curved surface, the same coil can be used for different animals. (b) Top view of the external array showing the coil layout in a 2 × 4 configuration. (c) Picture of the external array with individual FR4 circuit boards for each channel, with the tuning/matching network and floating bazooka baluns for each element in the 8-channel embedded array. (d) Close up view of the coil elements showing the bent wires where the loops are overlapped in the region indicated by the solid box in (c). (e) 8-channel external array loaded with a phantom and connected to the 8-channel preamplifier box.

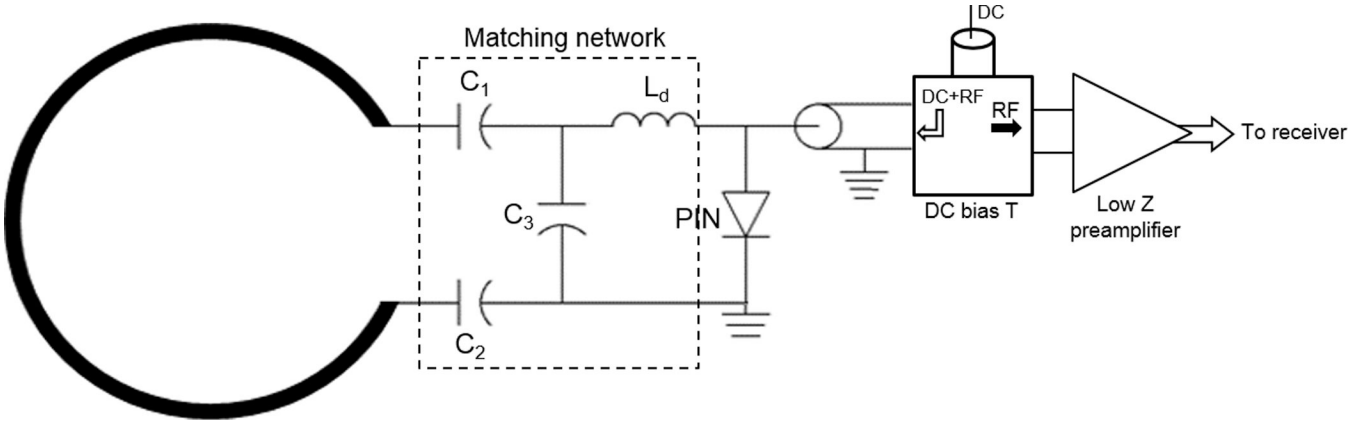

Figure 3.

Electrical scheme of a typical coil element used in the 8-channel embedded and external arrays. The electrical length of the RF cable was adjusted to provide 180° phase at the input of the preamplifier. The blocking circuit for detuning consisted of C_3 and L_d is activated by providing DC current to the PIN diode via a bias T located before the low-input impedance preamplifier.

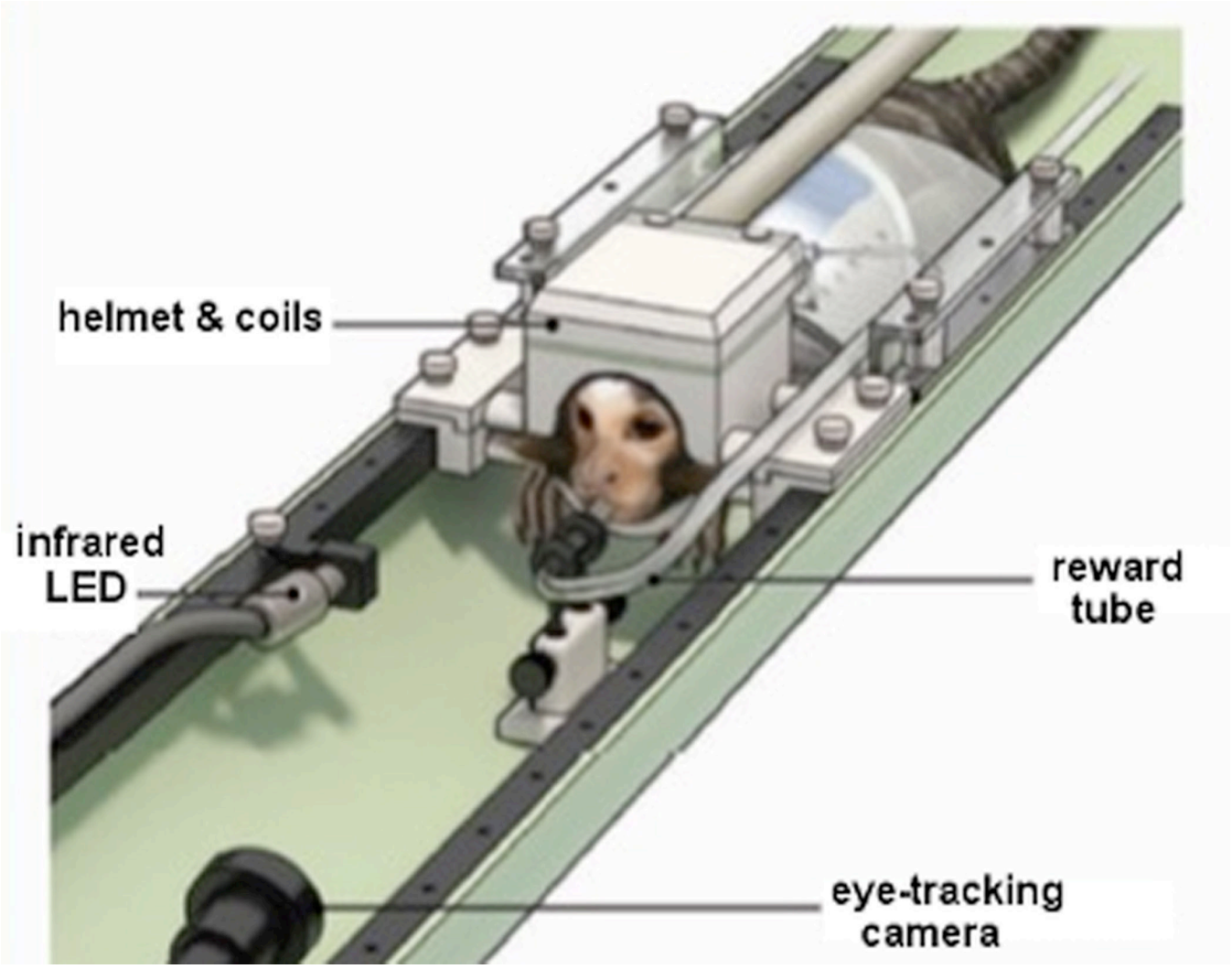

Figure 4.
Marmoset with the movement restraining helmet and the 8-channel embedded array, the eye-track camera and the rewarding system. Reprinted with permission from ref[31].

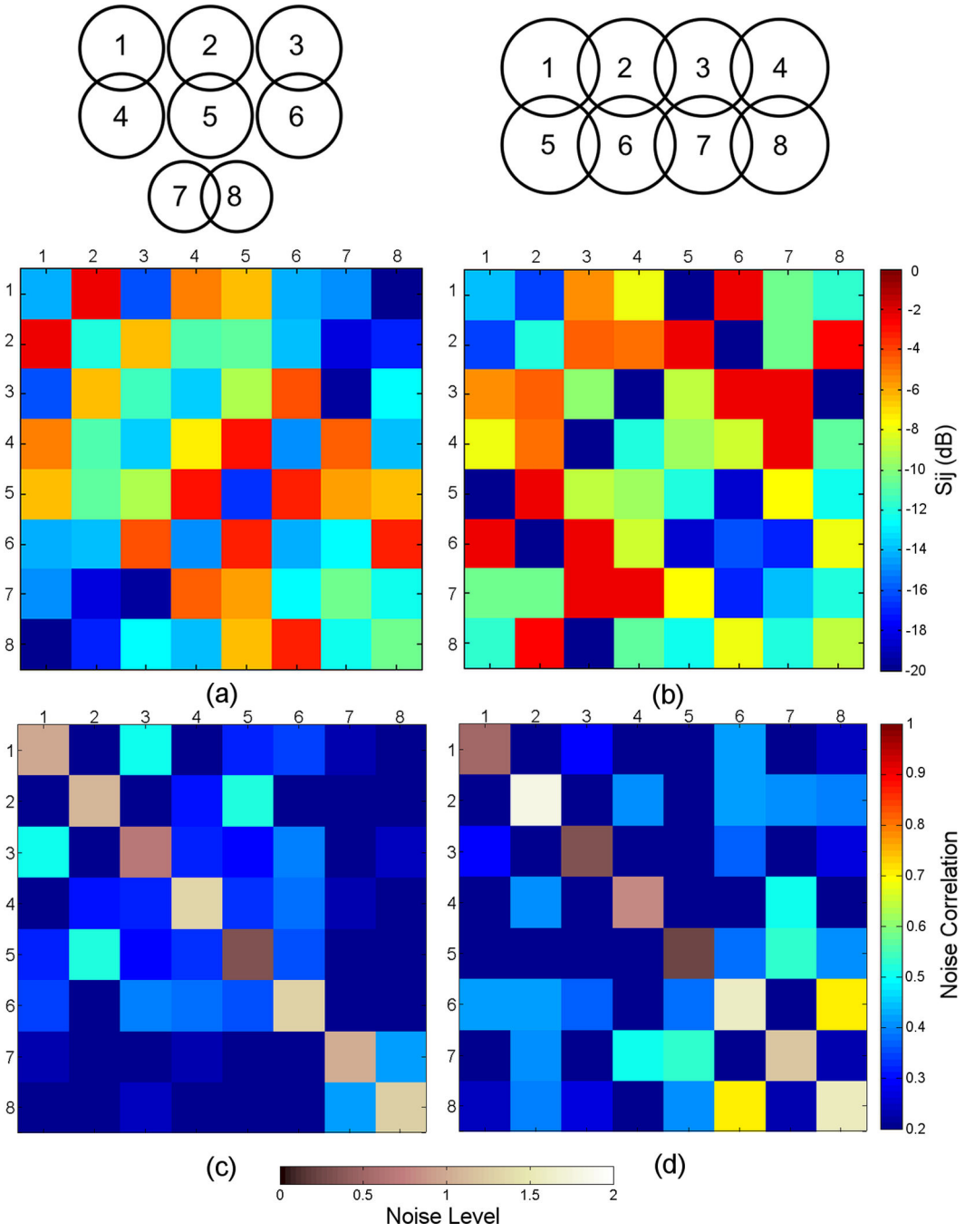

Figure 5.

S-parameter matrices measured directly with the network analyzer for (a) 8-channel embedded array. (b) 8-channel external array. Noise correlation matrices calculated from images acquired without RF excitation for (a) 8-channel embedded array. (b) 8-channel external array. The main diagonal of the matrices represent the distribution of noise level, which has been normalized to one.

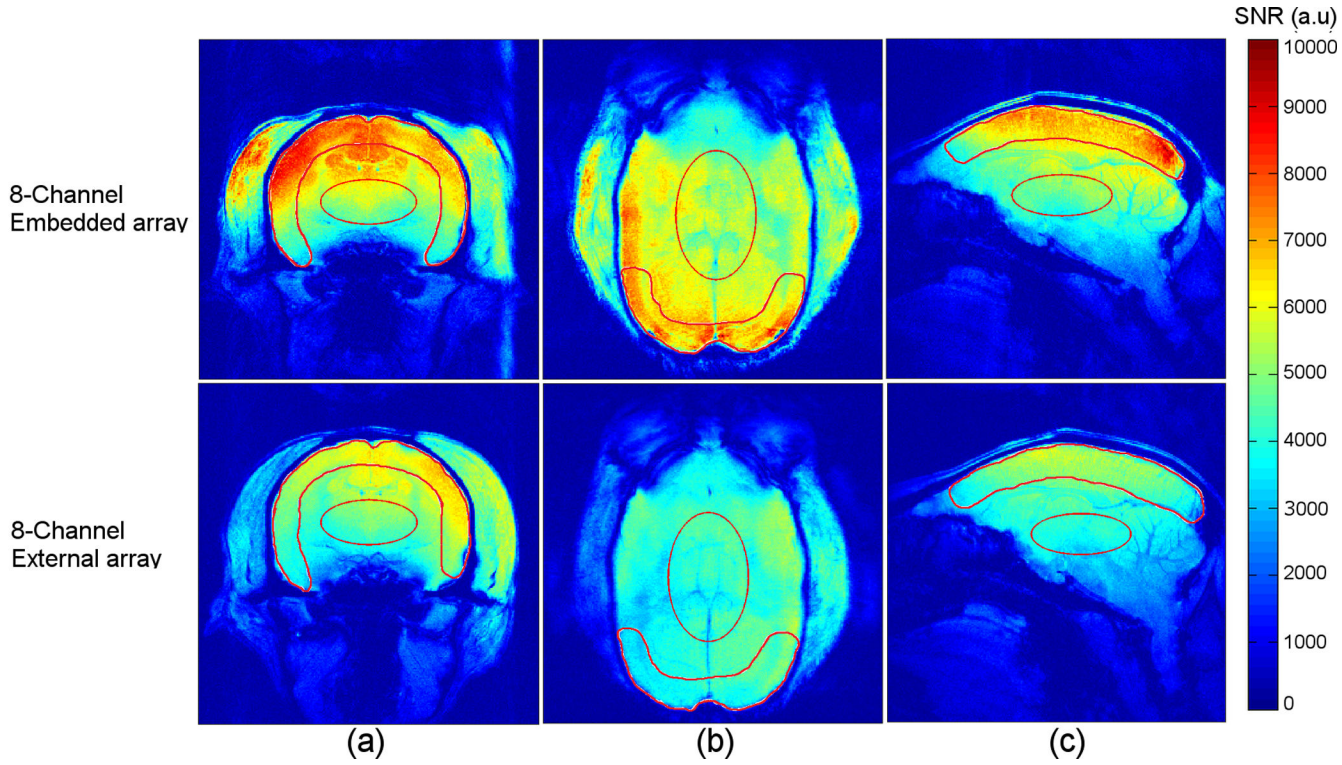

Figure 6.

SNR maps obtained in the axial (a), coronal (b) and sagittal (c) orientation from a conscious, awake marmoset using the 8-channel embedded array (top row) and the 8-channel external array (bottom row). The solid lines indicate ROIs for SNR measurements (see text).

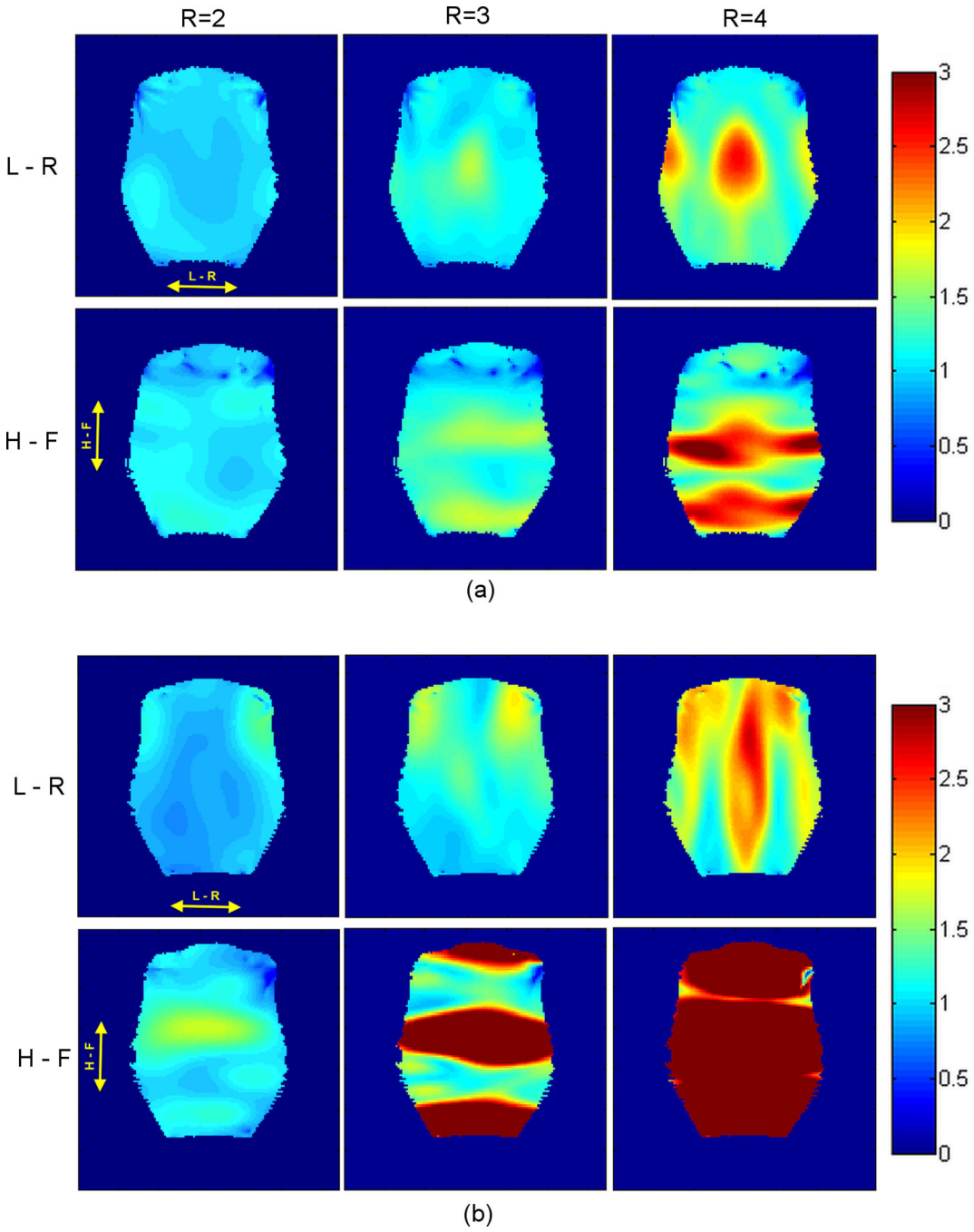

Figure 7.

G-factor maps acquired for R = 2, R = 3 and R = 4, with phase encoding direction left - right (L – R, top row) and head-foot (H – F, bottom row) using the 8-channel embedded array (a) and the 8-channel external coil (b). The images for g-factor maps calculation were acquired in coronal orientation in a plane located 20 mm from the inner surface of the helmets.

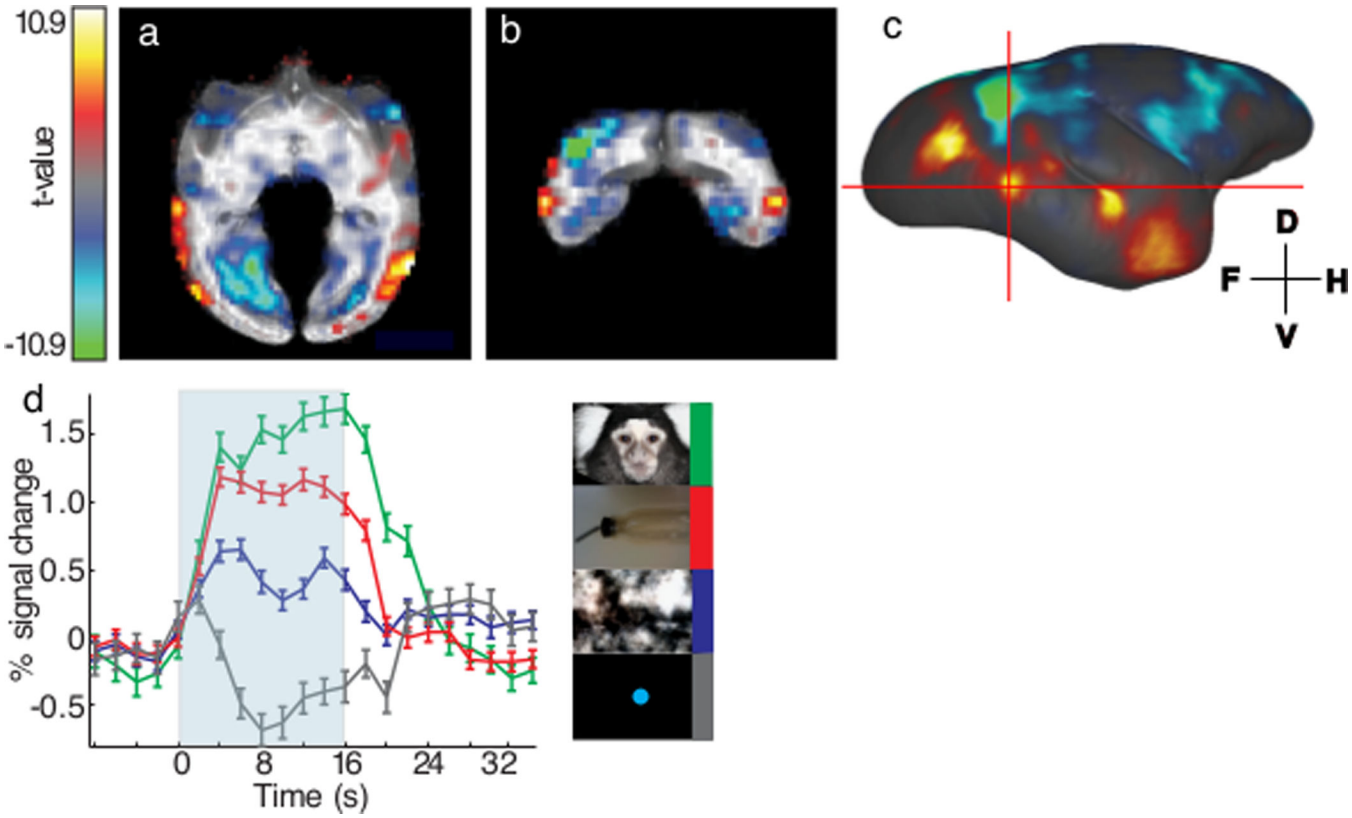

Figure 8.

BOLD fMRI activation maps and time courses of awake marmosets acquired using the 8-channel embedded arrays. Sub-figure (a) and (b) showed axial and coronal view of the fMRI statistical t-value map in the right hemisphere of one representative marmoset. Significant activation (face vs. object) could be detected in the occipitotemporal cortex. Color scale was ranging from t = 10.9 to t = −10.9 with alpha-channel (transparency) denoted the significance as well and no threshold was used. Area with red-yellow color meant higher BOLD response in face visual stimuli; area with blue-green color meant higher BOLD response in object visual stimuli. Activation map was further surface rendered to visualize the face patches in (c). Five distinct patches were discriminated with the upper-right one being the weakest and seemed discrete. The red crosshair represented two cross-sections of 8a and 8b. The intersection point was the center of one face patch and its time courses of four visual stimuli were plotted in (d). Voxels with t-value > 5 for the contrast between face and fixation dot were clustered together for averaging. BOLD response of four visual stimuli, faces (green), objects/body parts (red), spatial/frequency -scrambled face (blue), and fixation dot (gray), were plotted against 32-s period. Significant BOLD responses were observed in all visual stimuli for 16-s, except fixation dot, which only activated for a short period of time. Small (<0.5%), but significant, BOLD response difference between face and object/body parts visual stimuli was found in this face patch and was true for all other four face patches reported previously.

Table 1

G-factor values calculated for phantom images acquired in coronal orientation in a plane located 20 mm from the inner surface of the helmets

		R=2 (L-R)	R=3 (L-R)	R=4 (L-R)	R=2 (H-F)	R=3 (H-F)	R=4 (H-F)
8-Ch Embedded	**Mean**	1.00	1.13	1.47	1.05	1.25	1.76
	SD	0.06	0.15	0.36	0.09	0.24	0.62
	Max	1.17	1.65	2.62	1.20	1.74	3.33
8-Ch External	**Mean**	1.00	1.23	1.74	1.13	2.94	7.27
	SD	0.11	0.22	0.39	0.21	1.89	3.19
	Max	1.43	1.91	2.76	1.73	7.12	14.28